

# “Two-step” model of molecular diffusion in silicalite

Jörg Kärgner

*Fakultät für Physik und Geowissenschaften der Universität Leipzig, Linnéstraße 5,  
D-04103 Leipzig, Germany*

Pierfranco Demontis,<sup>a)</sup> Giuseppe B. Suffritti, and Antonio Tilocca

*Dipartimento di Chimica, Università degli Studi di Sassari, Via Vienna 2, I-07100 Sassari, Italy*

(Received 23 June 1998; accepted 22 September 1998)

The influence of the particle “memory” on long-range diffusion in the channel network of silicalite is taken into account by considering pairs of subsequent steps between the channel intersections. It is shown that in this case the correlation rule between the principal elements of the diffusion tensor has to be modified by including an additional term, which takes account of the deviation of molecular propagation from complete randomness. The obtained relations are discussed in terms of molecular dynamics simulations of ethane in silicalite. © 1999 American Institute of Physics. [S0021-9606(99)50401-7]

## I. INTRODUCTION

The confinement by the network of channels and/or pores in zeolitic adsorbate–adsorbent systems of noncubic structure may have the effect that intracrystalline molecular propagation in different directions is not independent from each other. Zeolite structures which may give rise to this type of correlated motion involve ZSM-5 (silicalite I), ZSM-11 (silicalite II), and chabazite.<sup>1–3</sup> Experimental evidence of this phenomenon, however, is difficult to provide. As a consequence of the small size of zeolite crystallites, the measurement of diffusion anisotropy either by transient uptake techniques<sup>4–6</sup> or by the pulsed field gradient (PFG) nuclear magnetic resonance (NMR) method<sup>7–9</sup> is subjected to substantial experimental uncertainty, which may be expected to be on the order of magnitude of the effects of correlated motion. Quantitatively, the effect of correlated motion results in an interdependence of the main elements of the diffusion tensor. For ZSM-5, e.g., the following relation has been derived:<sup>1,2</sup>

$$a^2/D_x + b^2/D_y = c^2/D_z, \quad (1)$$

where  $D_x$ ,  $D_y$ ,  $D_z$  and  $a$ ,  $b$ ,  $c$  denote the main elements of the diffusion tensor and the unit cell extensions in  $x$ ,  $y$  and  $z$  directions, respectively. Figure 1 schematically shows the structure of zeolite ZSM-5, where the full lines represent the axes of the zigzag channels (in the  $x$  direction) and of the straight channels (in the  $y$  direction), respectively. As a sole condition for deriving Eq. (1), molecular propagation from one channel intersection to the subsequent one has been assumed to be independent of the history of the given molecule. When a molecule enters an intersection, it will proceed to one of the four adjacent ones with a probability independent of the channel section from which it has come from. This assumption was not in conflict with the experimental data<sup>7–9</sup> and has been, moreover, supported by the evidence of molecular dynamics (MD) simulations<sup>10–12</sup> for

simple, spherical molecules like xenon and methane. For sufficiently long alkanes, however, as a consequence of the spatial extension of the molecule, molecular propagation from one channel intersection to the next one cannot be expected anymore to be independent of the trajectory. In these cases, clearly, substantial deviation from the correlation rule [Eq. (1)] must occur, which have been exemplified in recent molecular simulations.<sup>13,14</sup>

As a first approximation, the correlation between subsequent displacements from channel intersection to channel intersection (i.e., between the vertices in Fig. 1) may be taken into account by considering pairs of steps between subsequent channel intersections. The consequences of such a “two-step” model for long-range propagation and the correlation rule between the diffusivities in different directions shall be derived and compared with the results of MD simulations for ethane in silicalite. For this purpose, we used an extension to the random-walk model used in Ref. 1, which takes into account all possible “coupled” displacements among three succeeding intersections. An accurate and *explicit* calculation of the probability of each kind of event is carried out on the basis of MD trajectories. The simulations cover various cases in order to test the validity of the model and to gain insight into the diffusional mechanism of ethane under different conditions.

## II. THE TWO-STEP MODEL

In this model two subsequent (“single-step”) displacements between intersections are combined in a coupled (or “two-step”) event. There are basically three kinds of such coupled displacements: two steps in the straight channel, two steps in the zigzag channel or an interchange between straight and zigzag channels. Figure 1 shows examples for these three possibilities.

Let us look at the probabilities that, on its way through three subsequent intersections, a molecule crosses two straight channels ( $p_{ss}$ ), two zigzag channels ( $p_{zz}$ ), a straight

<sup>a)</sup>Electronic mail: demontis@ssmain.uniss.it

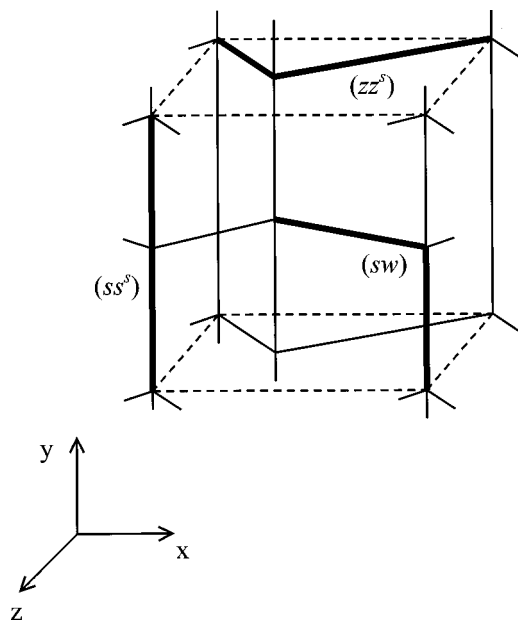


FIG. 1. Schematic representation of the channels geometry in a silicalite unit cell; channels are represented by continuous lines. The three main coupled displacements are shown as thick lines: ( $ss^s$ ), two displacements in straight channels, in the same  $y$  direction; ( $sw$ ), a switch from a straight to a zigzag channel, or vice versa; ( $zz^s$ ), two displacements in zigzag channels, in the same  $x$  direction.

channel followed by a zigzag one ( $p_{sz}$ ) or a zigzag channel followed by a straight one ( $p_{zs}$ ).

If the motion is uncorrelated, then these probabilities can be written as

$$p_{ss} = p_s^2 \quad p_{zz} = p_z^2 \quad p_{sz} = p_{zs} = p_s p_z, \quad (2)$$

which obviously obey the condition:

$$p_{ss} + p_{zz} + p_{sz} + p_{zs} = (p_s + p_z)^2 = 1. \quad (3)$$

$p_s$  and  $p_z$  are the single-step probabilities that the molecule exit from an intersection to a straight channel or to a zigzag one, respectively. Note that the coupled displacements in the straight or zigzag channels could be both in the same direction ( $p_{ss}^s$  and  $p_{zz}^s$ ) or in opposite directions ( $p_{ss}^o$  and  $p_{zz}^o$ ): in this last case the first and the third intersections are identical, i.e., the molecule returns to the starting intersection after having visited a neighboring one. Obviously,  $p_{ss} = p_{ss}^s + p_{ss}^o$ , and  $p_{zz} = p_{zz}^s + p_{zz}^o$ .

If we want to express the components  $\langle \Delta x^2(t) \rangle$ ,  $\langle \Delta y^2(t) \rangle$  and  $\langle \Delta z^2(t) \rangle$  of the mean square displacement as a function of the measured numbers of coupled displacements, it is very important to distinguish between the coupled displacements in the same and in opposite directions. These last events do not take part in the overall motion of the molecule. Moreover, as visible from Fig. 1, the total displacement during one two-step event clearly depends on the individual steps: two displacements in the *same* zigzag direction lead to a displacement of  $a$  along  $x$  ( $a/2$  being the distance between two intersections along the zigzag channel, i.e., the length of each single step); two displacements in the *same* straight direction lead to a displacement of  $b$  along  $y$  ( $b/2$  being the distance between two intersections along the straight chan-

nel); finally, each switch event (with probability  $p_{sw} = p_{sz} + p_{zs}$ ) leads to displacements of  $a/2$ ,  $b/2$  and  $c/2$  along  $x$ ,  $y$  and  $z$  directions, respectively. This happens because an  $a/2$  displacement followed by a  $b/2$  one (or vice versa) necessarily implies a  $c/2$  displacement along the  $z$  direction. Therefore, the correct expressions for the monodimensional mean square displacements (MSD) should be

$$\langle \Delta x^2(t) \rangle = n_{zz}^s(t) a^2 + n_{sw}(t) (a/2)^2, \quad (4)$$

$$\langle \Delta y^2(t) \rangle = n_{ss}^s(t) b^2 + n_{sw}(t) (b/2)^2, \quad (5)$$

$$\langle \Delta z^2(t) \rangle = n_{sw}(t) (c/2)^2, \quad (6)$$

where the  $n(t)$ s are the numbers of coupled events detected in an observation time  $t$ . The correctness of these expressions may be verified by showing their coincidence with the correlation rule for random propagation. For this purpose, we express the numbers of coupled events as a function of the numbers  $n_s$  and  $n_z$  of single steps. In the case of random propagation, we have  $p_{zz}^s = p_{zz}^o$  (any difference between  $p_{zz}^s$  and  $p_{zz}^o$  indicates deviations from strict randomness). Note that in the following the time dependency of the  $n$  event numbers will not be explicitly indicated, therefore  $n$  should be read  $n(t)$ , and so on.

From Eq. (2) we find

$$p_{zz} = p_{zz}^s + p_{zz}^o \underset{\text{(random case)}}{=} 2p_{zz}^s = 2p_{zz}^o, \quad (7)$$

hence

$$p_{zz}^s = p_{zz}^o = \frac{1}{2} p_z^2 = \frac{1}{2} (n_z/n)^2. \quad (8)$$

We may use the notation

$$p_{zz}^s = n_{zz}^s/n_2, \quad (9)$$

where  $n_2 = n_{ss} + n_{zz} + n_{sw}$  is the total number of coupled steps. It is equal to *one half* of the total number  $n$  of single steps, because every coupled event is composed of *two* single steps

$$n = 2n_2. \quad (10)$$

Thus, from Eqs. (8), (9) and (10),

$$n_{zz}^s = n_{zz}^o = \frac{1}{4} n_z^2/n. \quad (11)$$

With analogous calculations, one obtains

$$n_{ss}^s = n_{ss}^o = \frac{1}{4} n_s^2/n. \quad (12)$$

On the other hand, we can write:

$$p_{sw} = p_{sz} + p_{zs} \underset{\text{(random case)}}{=} 2p_{sz} = 2p_{zs} = 2p_s p_z, \quad (13)$$

hence

$$n_{sw}/n_2 = 2n_s n_z/n^2, \quad (14)$$

and finally:

$$n_{sw} = n_s n_z/n. \quad (15)$$

Substituting in Eqs. (4)–(6) the quantities  $n_{zz}^s$ ,  $n_{ss}^s$  and  $n_{sw}$  by the relations (11), (12) and (15) as resulting for random propagation from intersection to intersection, one obtains

$$\langle \Delta x^2(t) \rangle = n_z (a/2)^2, \quad (16)$$

$$\langle \Delta y^2(t) \rangle = n_s (b/2)^2, \quad (17)$$

$$\langle \Delta z^2(t) \rangle = n_s n_z / n (c/2)^2. \quad (18)$$

From Eqs. (16)–(18) we find

$$\begin{aligned} & \frac{a^2}{4\langle \Delta x^2(t) \rangle} + \frac{b^2}{4\langle \Delta y^2(t) \rangle} \\ &= \frac{1}{n_z} + \frac{1}{n_s} \\ &= \frac{n}{n_s n_z} = \frac{c^2}{4\langle \Delta z^2(t) \rangle}, \end{aligned} \quad (19)$$

which, due to

$$\begin{aligned} \langle \Delta x^2(t) \rangle &= 2D_x t; & \langle \Delta y^2(t) \rangle &= 2D_y t; \\ \langle \Delta z^2(t) \rangle &= 2D_z t \end{aligned} \quad (20)$$

is nothing more than the correlation rule, Eq. (1).

To derive the equivalent of the correlation rule, Eq. (1), for molecular propagation with non-negligible memory, we introduce the quantities

$$\Delta n_{zz}^s = n_{zz}^s - \frac{1}{4} n_z^2 / n, \quad (21a)$$

$$\Delta n_{zz}^o = n_{zz}^o - \frac{1}{4} n_z^2 / n, \quad (21b)$$

$$\Delta n_{ss}^s = n_{ss}^s - \frac{1}{4} n_s^2 / n, \quad (22a)$$

$$\Delta n_{ss}^o = n_{ss}^o - \frac{1}{4} n_s^2 / n, \quad (22b)$$

$$\Delta n_{sw} = n_{sw} - n_s n_z / n, \quad (23)$$

representing the deviations of the actual number of two-step events of a certain type from that of the completely random case, as provided by Eqs. (11), (12) and (15). By introducing Eqs. (21)–(23), Eqs. (4)–(6) may be transferred into

$$\langle \Delta x^2(t) \rangle = \frac{1}{4} a^2 (n_z + 4\Delta n_{zz}^s + \Delta n_{sw}), \quad (24)$$

$$\langle \Delta y^2(t) \rangle = \frac{1}{4} b^2 (n_s + 4\Delta n_{ss}^s + \Delta n_{sw}), \quad (25)$$

$$\langle \Delta z^2(t) \rangle = \frac{1}{4} c^2 (n_s n_z / n + \Delta n_{sw}), \quad (26)$$

or

$$\frac{a^2}{4\langle \Delta x^2(t) \rangle} = \frac{1}{n_z + 4\Delta n_{zz}^s + \Delta n_{sw}} \approx \frac{1}{n_z} - \frac{4\Delta n_{zz}^s}{n_z^2} - \frac{\Delta n_{sw}}{n_z^2}, \quad (27)$$

$$\frac{b^2}{4\langle \Delta y^2(t) \rangle} = \frac{1}{n_s + 4\Delta n_{ss}^s + \Delta n_{sw}} \approx \frac{1}{n_s} - \frac{4\Delta n_{ss}^s}{n_s^2} - \frac{\Delta n_{sw}}{n_s^2}, \quad (28)$$

$$\frac{c^2}{4\langle \Delta z^2(t) \rangle} = \frac{1}{\frac{n_s n_z}{n} + \Delta n_{sw}}$$

$$\approx \frac{1}{n_z} + \frac{1}{n_s} - \Delta n_{sw} \left( \frac{1}{n_s^2} + \frac{1}{n_z^2} + \frac{2}{n_s n_z} \right), \quad (29)$$

where we have made use of the fact that  $n_z + n_s = n$  [Eq. (10)] and that—as a first approximation—the deviations  $\Delta n_{zz}^s$ ,  $\Delta n_{ss}^s$  and  $\Delta n_{sw}$  are small in comparison with  $n_z$  and  $n_s$  [in particular, we assumed that:  $n_z \gg (4\Delta n_{zz}^s + \Delta n_{sw})$  in Eq.

(27);  $n_s \gg (4\Delta n_{ss}^s + \Delta n_{sw})$  in Eq. (28);  $n_s n_z \gg n \Delta n_{sw}$  in Eq. (29)]. We verified that the approximation is excellent for Eq. (28), while the errors are between 5% and 15% for the approximated Eqs. (27) and (29), compared with their exact forms. For example, from Tab. III and VII, for 4 ethane/u.c. at 300 K, one obtains:  $(4\Delta n_{zz}^s + \Delta n_{sw})/n_z = -0.38$ ;  $(4\Delta n_{ss}^s + \Delta n_{sw})/n_s = -0.02$ ;  $n \Delta n_{sw} / (n_s n_z) = -0.38$ .

Combining Eqs. (27)–(29) yields

$$\begin{aligned} \frac{a^2}{4\langle \Delta x^2(t) \rangle} + \frac{b^2}{4\langle \Delta y^2(t) \rangle} &\approx \frac{c^2}{4\langle \Delta z^2(t) \rangle} - \frac{4\Delta n_{zz}^s}{n_z^2} - \frac{4\Delta n_{ss}^s}{n_s^2} \\ &+ \frac{2\Delta n_{sw}}{n_s n_z}, \end{aligned} \quad (30)$$

hence via Eqs. (20)

$$\frac{a^2}{D_x} + \frac{b^2}{D_y} \approx \frac{c^2}{D_z} - \frac{32\Delta n_{zz}^s}{n_z \cdot (n_z/t)} - \frac{32\Delta n_{ss}^s}{n_s \cdot (n_s/t)} + \frac{16\Delta n_{sw}}{n_s n_z / t}. \quad (31)$$

Finally, combining Eqs. (16)–(18) with Eqs. (20), in first order approximation the quantities  $n_z/t$  and  $n_s/t$  on the right side of Eq. (31) may be replaced by  $8D_x/a^2$  and  $8D_y/b^2$ , respectively, while the quantity  $n_s n_z/t$  may be replaced by  $8nD_z/c^2$ . Thus one obtains the generalized correlation rule

$$\frac{a^2}{D_x} \left( 1 + \frac{4\Delta n_{zz}^s}{n_z} \right) + \frac{b^2}{D_y} \left( 1 + \frac{4\Delta n_{ss}^s}{n_s} \right) = \frac{c^2}{D_z} \left( 1 + \frac{2\Delta n_{sw}}{n} \right). \quad (32)$$

Equation (32) quantitatively relates the diffusivities in the  $x$  and  $y$  direction to the diffusivity in the  $z$  direction, if subsequent displacements between the channel intersections are correlated. As to be expected, any preferential continuation of propagation in the same type of channel segment, which—according to Eqs. (21) and (22)—corresponds to positive  $\Delta n_{zz}^s$  and  $\Delta n_{ss}^s$  values, leads to a decrease in  $D_z$  in comparison with the prediction of the correlation rule [Eq. (1)], for completely random propagation. Moreover, any preferential tendency to switch channel segment, entailing positive  $\Delta n_{sw}$  values, leads to an increase of  $D_z$  in comparison with the value predicted by Eq. (1). It is doubtless a challenging task of further research to use Eq. (32) for studying correlation effects in molecular dynamics on the basis of experimental data on diffusion anisotropy.

In the following, the potentials of Eqs. (4)–(6) for quantitatively predicting molecular propagation patterns in silicalite shall be investigated by MD simulations.

### III. SIMULATIONS

The simulation box consisted of two silicalite unit cells (cf. Fig. 1) superimposed along  $z$  (the unit cell edges were  $a = 20.022 \text{ \AA}$ ,  $b = 19.899 \text{ \AA}$ ,  $c = 13.383 \text{ \AA}$ ), resulting in 576 framework atoms (192 Si and 384 O). The full flexibility of the silicalite lattice was accounted for by a harmonic model, described in detail in Refs. 15 and 16. Ethane is modeled by two point sites representing methyl groups, the site-to-site intermolecular potential being of the Lennard-Jones form;

the intramolecular interaction is represented with a Morse potential. The intra and intermolecular parameters adopted are reported in Ref. 17.

Four MD simulations at 300 K have been carried out, with 1, 2, 4 and 6 ethane molecules per unit cell. The equilibration run length was 400 ps, during which the atom velocities, starting from zero, were adequately rescaled to achieve the desired temperature. Having previously<sup>17</sup> established that a 3 ns "production" run with 4 ethane molecules per unit cell gave a good statistical accuracy, we extended the length of the trajectories with lower loadings to 12 ns for 1 ethane/u.c., and to 6 ns for 2 ethane/u.c., in order to obtain a reasonably accurate sampling of the phase space in all cases. Another two simulations of 3 ns at 400 and 500 K were carried out with 4 molecules/u.c. The center of mass coordinates of ethane molecules were stored every 32 fs.

#### IV. TRAJECTORIES ANALYSIS

The analysis of the motion is based on an accurate mapping of the different zones in which the micropores of silicalite can be divided; the projection of a trajectory in the  $xy$  plane [Fig. 2(a), run at 500 K] shows that the various zones (straight channels, zig-zag channels and intersections) are well defined using only these two coordinates. The  $xy$  plane was then divided into:

- straight channel sections: rectangles with edges 5.2 Å (along  $y$ ) and 4.8 Å (along  $x$ ) centered at  $x=0, \pm 10, \pm 20, \dots$  and  $y=0, \pm 10, \pm 20, \dots$ ,
- zig-zag channel sections (whose  $xy$  projection is actually *straight*): rectangles with edges 5.2 Å (along  $x$ ) and 4.8 Å (along  $y$ ), centered at  $x=\pm 5, \pm 15, \pm 25, \dots$  and  $y=\pm 5, \pm 15, \pm 25, \dots$ ,
- intersections between two orthogonal channels: squares with edges of 4.8 Å, centered at  $x=0, \pm 10, \pm 20, \dots$  and  $y=\pm 5, \pm 15, \pm 25, \dots$ .

The division is sketched in Fig. 2(b), in which a part of Fig. 2(a) is enlarged, and the intersection region centered at  $(x=0, y=-5)$  is shown. It must be remarked that the channel sections are often considered longer than 5.2 Å, and the width of the intersections, projected on the plane, can be lower than 4.8 Å. But, looking at the  $xy$  projection of our trajectories, we found this division more suitable to describe them; indeed, in our case, it is very important to know when a particle reaches or leaves an intersection (see below), and with shorter intersection edges some cases would not have been correctly considered. Moreover, the probability of two-step events of opposite direction clearly increases with larger extension of the considered intersection range (we verified that this is mainly valid for the straight channel, while the effect is much smaller for the zigzag channel whose peculiar topology considerably hinders a molecule from continuing in the same  $x$  direction). In this way, the benefit of the generalized correlation rule, Eq. (32), in comparison with Eq. (1) should become more pronounced.

In the  $xy$  plane every intersection could then be identified as a couple of integers  $(n, m)$  corresponding to the intersection center, expressed in Å. The path of a molecule is described in terms of the succession of *different* intersections

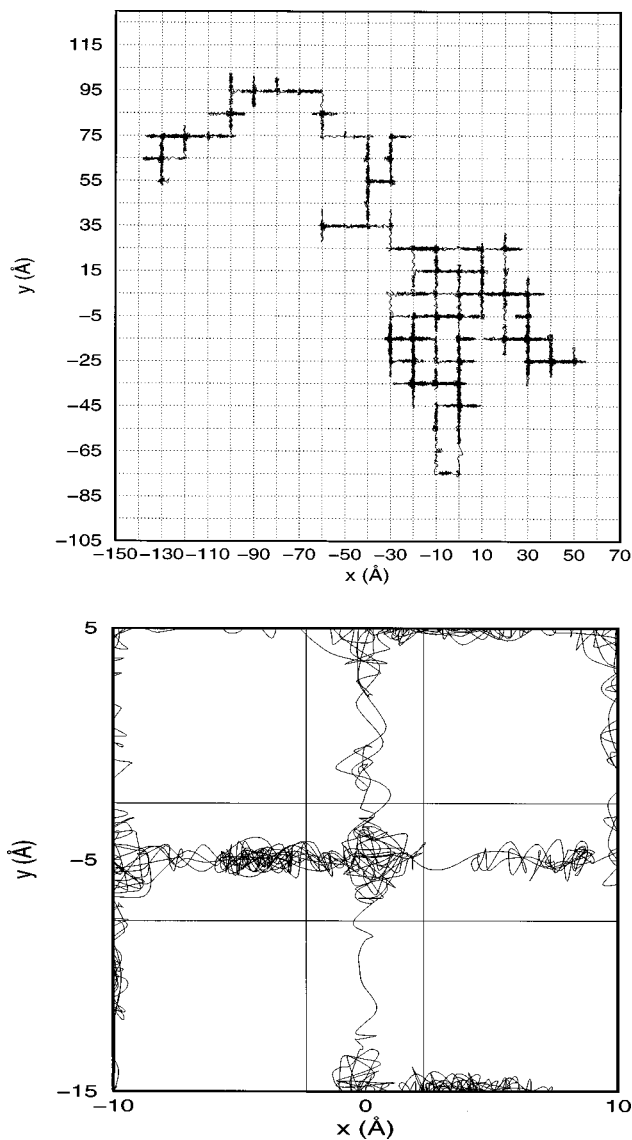


FIG. 2. Projection on the  $xy$  plane of the trajectory of an ethane molecule in silicalite (trajectory length: 3 ns,  $T=500$  K). (b) Enlargement of a part of (a), showing in detail the intersection region centered at  $x=0, y=-5$ .

reached, i.e., in terms of the corresponding sequence of  $(n, m)$  pairs. This sequence is then analyzed starting from the first intersection, and establishing what kind of coupled displacement has led the molecule to the second and then to the third intersection; this step is then repeated starting from the second intersection in the series, and so on. Results are averaged over all molecules. The number and the duration of each kind of single and two-step displacements found are recorded and averaged. Note that *all* subsequent intersections are taken as origins in order to achieve the best statistics possible. But the applications of the two-step model, which is based on jumps from the first to the third intersection, then from the third to the fifth one, and so on, requires that the event numbers calculated in this way must be divided by two.

Some errors could stem from the application of the geometrical criterion described above to these trajectories. The conservation of the total linear momentum of our system

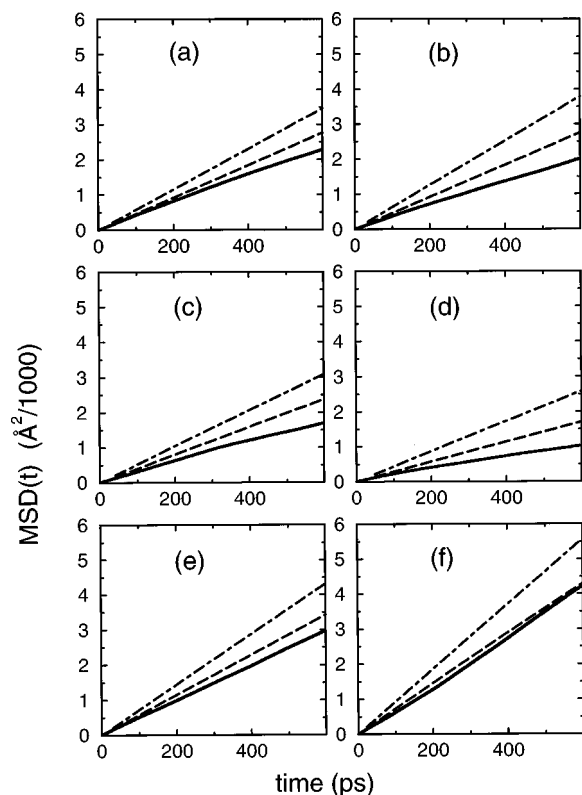


FIG. 3. Mean square displacement curves obtained according to the two-step model (dashed line), one-step model (dot-dashed line) and Eq. (5) (solid line): (a)  $T=300$  K, 1 molecule/u.c.; (b)  $T=300$  K, 2 molecule/u.c.; (c)  $T=300$  K, 4 molecule/u.c.; (d)  $T=300$  K, 6 molecule/u.c.; (e)  $T=400$  K, 4 molecule/u.c.; (f)  $T=500$  K, 4 molecule/u.c.

(which is zero, as the initial velocities are) leads to a resulting nonzero linear momentum for the framework. This momentum, albeit small, results in a slow translational motion of the whole framework, which does not much affect the values of the diffusion coefficients and other dynamical variables, but could be very important when the coordinates of the particles are mapped on the basis of the *initial* position of the framework, as in the present case. For example, after 3 ns, we found in some cases displacements of 2–3 Å of the  $x$  coordinate of *all* framework atoms compared to the starting values, indicating a slow overall translational motion along  $x$  (obviously, the displacement could also be observed in other directions). We solved this problem by referring the stored coordinates of the guest particles to the initial position of the framework center of mass, i.e., before the storage, the position vectors  $\mathbf{r}_i$  were scaled as

$$\mathbf{r}_i(t) = \mathbf{r}_i(t) - \Delta \mathbf{r}_{\text{cm},f}(t), \quad (33)$$

where  $i$  stands for the guest particles, and  $\Delta \mathbf{r}_{\text{cm},f}(t)$  is the difference between the position of the framework center of mass at time  $t$  and its initial position, at  $t=0$ . The trajectories obtained in this way are then suitable for the right application of the geometrical mapping criterion, because the motion of the particles is always referred to the same (initial) geometry of the framework. Note that this correction leads to slight variations in the calculated diffusion coefficients compared to the values previously obtained for the same system without the correction for the framework motion.<sup>17</sup> It should

TABLE I. Diffusion coefficients at different loadings ( $/10^{-9} \text{ m}^2 \text{ s}^{-1}$ ).

Loading (molecule/u.c.)		$D$	$D_x$	$D_y$	$D_z$	$\frac{1}{2}(D_x + D_y)/D_z$
1	a	6.9	5.7	13.1	1.8	5.2
	b	7.6	8.6	12.2	2.1	4.9
	c	9.6	13.4	12.4	2.9	4.4
2	a	5.3	5.7	8.3	2.0	3.5
	b	7.6	8.2	12.6	2.0	5.2
	c	10.4	14.3	13.8	3.2	4.4
4	a	5.3	5.5	9.1	1.2	6.3
	b	6.7	7.6	10.7	1.6	5.7
	c	8.7	12.4	11.0	2.7	4.3
6	a	3.0	2.9	5.3	0.7	6.0
	b	4.8	5.1	7.9	1.3	5.0
	c	7.2	10.0	9.4	2.2	4.4

<sup>a</sup>Values obtained by the standard method [Eq. (34)].

<sup>b</sup>Values obtained according to the two-step model [Eqs. (4)–(6)].

<sup>c</sup>Values obtained according to the one-step model [Eqs. (16)–(18)].

be noted that in Eqs. (4)–(6) the time dependence of the monodimensional MSDs is associated with the time dependence of  $n_{zz}^s$ ,  $n_{ss}^s$  and  $n_{sw}^s$ . One simple but inaccurate way to proceed could be to calculate the  $n_{zz}^s$ ,  $n_{ss}^s$  and  $n_{sw}^s$  values from the full trajectory (averaging over all molecules); then the  $t$  value will be equal to the trajectory length  $\tau_{\text{RUN}}$ . But some inaccuracy stems from the fact that only one trajectory would be considered in each case, and moreover the time evolution of the MSDs could not be followed in this way. It is more interesting to study the time evolution of the MSDs as calculated by Eqs. (4)–(6), in order to better assess their validity by comparison with the values obtained through the standard method, i.e.,

$$\Delta r^2(t) = \frac{1}{N_0 N} \sum_{t_0=1}^{N_0} \sum_{i=1}^N |\mathbf{r}_i(t_0+t) - \mathbf{r}_i(t_0)|^2, \quad (34)$$

where the  $\mathbf{r}_i$ s are the center of mass coordinates of ethane molecules, and the average is over  $N$  molecules and  $N_0$  time origins.

The MSD obtained by Eq. (34) [which should obviously be compared with the *sum* of Eqs. (4)–(6)] is in the present case a sort of “experimental” value useful to test the theoretical model presented. Moreover, if the single-event numbers  $n_s$  and  $n_z$  are also calculated as a function of the time, the reliability of Eqs. (16)–(18) could also be evaluated. The

TABLE II. Diffusion coefficients at different temperatures ( $/10^{-9} \text{ m}^2 \text{ s}^{-1}$ ).

$T$ (K)		$D$	$D_x$	$D_y$	$D_z$	$\frac{1}{2}(D_x + D_y)/D_z$
300	a	5.3	5.5	9.1	1.2	6.3
	b	6.7	7.6	10.7	1.6	5.7
	c	8.7	12.4	11.0	1.7	4.3
400	a	8.0	7.7	14.7	1.5	7.5
	b	9.6	11.2	15.1	2.5	5.3
	c	12.0	16.7	15.7	3.7	4.4
500	a	11.0	8.1	22.5	2.3	6.7
	b	12.1	13.8	19.1	3.4	4.8
	c	15.4	19.9	21.7	4.8	4.3

<sup>a</sup>Values obtained by the standard method [Eq. (34)].

<sup>b</sup>Values obtained according to the two-step model [Eqs. (4)–(6)].

<sup>c</sup>Values obtained according to the one-step model [Eqs. (16)–(18)].

TABLE III. Event numbers (probabilities) per molecule at different loadings ( $t = 1$  ns).

Loading (molecule/u.c.)	$n_s$	$n_z$	$n_{ss}^s$	$n_{ss}^o$	$n_{zz}^s$	$n_{zz}^o$	$n_{sw}$	$n_{sz}$	$n_{zs}$	$n_1$	$n_2$
1	26.53 (0.501)	26.46 (0.499)	4.16 (0.157)	4.44 (0.168)	1.98 (0.075)	6.58 (0.248)	9.32 (0.352)	4.66 (0.176)	4.65 (0.176)	53.0	26.5
2	29.97 (0.507)	29.02 (0.492)	4.60 (0.156)	5.84 (0.198)	1.86 (0.063)	8.11 (0.275)	9.07 (0.307)	4.53 (0.154)	4.53 (0.154)	59.0	29.5
4	23.04 (0.48)	24.95 (0.52)	3.78 (0.157)	4.05 (0.169)	1.99 (0.083)	6.79 (0.283)	7.37 (0.307)	3.68 (0.154)	3.68 (0.153)	48.0	24.0
6	19.78 (0.494)	20.21 (0.506)	2.77 (0.139)	4.20 (0.21)	1.09 (0.055)	6.10 (0.305)	5.82 (0.291)	2.91 (0.145)	2.91 (0.145)	40.0	20.0

time dependence of the event numbers can be deduced by calculating the average number of each kind of event observed in a time  $t_0$  going from 0 to  $\tau_{\text{RUN}}$ , where  $\tau_{\text{RUN}}$  is the full trajectory length. When  $t_0 < \tau_{\text{RUN}}$  there will be a large number of time intervals of such length in the trajectory, and an accurate average can be made over all such intervals. In other words all the intervals of the “right” length  $t_0$  present in the trajectory of each molecule are taken into account in the calculation of the numbers of interest (such as  $n_{zz}^s$ , etc.), which will represent the number of events observed in  $t_0$ . Note that every time a specific event is observed, its duration is also recorded, so that the time evolution of the characteristic durations of each event could be observed. The statistical accuracy of the calculated numbers and timelengths is clearly improved with this method, because it corresponds to the evaluation of a large number of trajectories instead of only one. As for a typical correlation functions calculation, the number of trajectories accounted for decreases with increasing time, becoming one for  $t = \tau_{\text{RUN}}$ , and the statistical accuracy becomes worse.

## V. RESULTS AND DISCUSSION

### A. Direct calculation of diffusion coefficients by one- and two-step models

In Fig. 3 the three mean square displacement curves calculated according to Eqs. (4)–(6) (two-step model), Eqs. (16)–(18) (one-step model) and Eq. (34) (standard MSD calculation) are shown for each case studied here. It is immediately clear that both the diffusion models considered always overestimate the MSD with respect to the standard value obtained from Eq. (34). At the same time, it is evident that the two-step model always gives a good estimate of the mean square displacement: actually this model only slightly overestimates the “real” MSD value in its linear region (80–240 ps), whose slope was chosen to measure the diffusion coef-

ficient values. The agreement seems to improve at higher temperatures: at 500 K [Fig. 3(f)] the two curves are very close. It is interesting to note that the curves calculated according to Eqs. (4)–(6) and Eqs. (16)–(18) always show a very linear trend, also at longer times than those shown, while the MSD calculated by Eq. (34) is more sensitive to the higher statistical inaccuracy with increasing correlation time, showing a less linear trend at longer times, as it is already evident from Fig. 3.

The diffusion coefficients obtained from a linear fit to the real MSD curves calculated by Eq. (34) in the 80–240 ps region are reported in Tables I and II, indicated by the (a) notation. There is only a slight decrease with increasing loading from 1 to 4 ethane molecules/unit cell, while a net decrease is observed going to 6 molecules/u.c. Longer simulation runs, also with intermediate and higher loadings, would probably help to better elucidate this trend. The “anomalous” behavior observed for the 2 molecules/u.c. simulation (see below) emerges also when the anisotropy factor  $\frac{1}{2}(D_x + D_y)/D_z$  is calculated.<sup>1</sup> All studied cases give values greater than 4.4 (in agreement with the random walk model), except that with 2 molecules/u.c. The increase with the temperature was already accounted for in a previous paper,<sup>17</sup> where the Arrhenius parameters for the diffusion process were calculated and discussed. More information could be obtained looking again at Tables I and II, where the diffusion coefficients obtained from the MSDs calculated by the models are also reported. The (b) and (c) notations indicate values obtained from the two- and one-step model, respectively. The main source of error for the one-step model appears to be the far too high value of  $D_x$ , which is even slightly higher than the corresponding  $D_y$  value in almost all cases. Indeed, the  $D_y$  values obtained according to the two models are always similar. The diffusional anisotropy characteristic of silicalite, which should lead to  $D_y$  values signifi-

TABLE IV. Event numbers (probabilities) per molecule at different temperatures ( $t = 1$  ns).

T(K)	$n_s$	$n_z$	$n_{ss}^s$	$n_{ss}^o$	$n_{zz}^s$	$n_{zz}^o$	$n_{sw}$	$n_{sz}$	$n_{zs}$	$n_1$	$n_2$
300	23.04 (0.48)	24.95 (0.52)	3.78 (0.157)	4.05 (0.169)	1.99 (0.083)	6.79 (0.283)	7.37 (0.307)	3.68 (0.154)	3.68 (0.153)	48.0	24.0
400	32.721 (0.495)	33.279 (0.505)	4.935 (0.149)	5.858 (0.177)	2.862 (0.087)	8.209 (0.249)	11.135 (0.337)	5.568 (0.169)	5.567 (0.169)	66.0	33.0
500	46.466 (0.534)	40.534 (0.466)	6.099 (0.140)	9.249 (0.213)	2.861 (0.066)	9.521 (0.219)	15.770 (0.363)	7.881 (0.181)	7.889 (0.182)	87.0	43.5

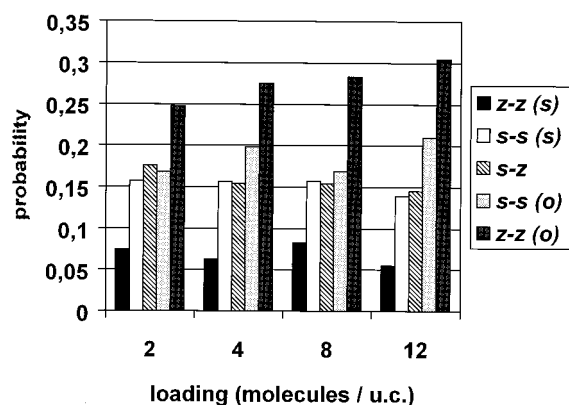


FIG. 4. Histograms of the event probabilities at different loadings ( $T = 300$  K).

cantly greater than  $D_x$ , is not reproduced at all with the direct application of Eqs. (16)–(18).

Tables III and IV report the numbers of single- and two-step events found in the simulations, together with their respective probabilities. The last two columns report the total numbers of single steps and two steps recorded. In order to compare each other with the event numbers, the values obtained for  $t = 1$  ns have been listed. This choice of  $t$  is not crucial for a comparison of the results, due to the very linear trend of the MSD curves calculated by Eqs. (4)–(6) and Eqs. (16)–(18). It could be argued that the reported numbers of events are rather small; actually, if we increased the “observation time”  $t$ , we would obtain greater numbers, but affected by higher errors, due to the lower number of time intervals of duration  $t$  included in the average. For example, if we took  $t = 3$  ns for the 4 ethane/u.c. case, we would obtain the largest event numbers possible ( $t$  being equal to the full trajectory length) but at the same time they would be considerably inaccurate (having been computed from a *single* time interval). The accuracy of the numbers obtained with  $t = 1$  ns is doubtless better, with the present trajectory length. In order to record as many events as possible, also with good statistical accuracy, very long trajectories would be needed, but this would also require prohibitive calculation times.

Looking at Tables III and IV, it is interesting to observe the *total* number of events ( $n_1$  or  $n_2$ ). While, on one hand, these numbers obviously increase with temperature, on the other hand the trend with different loadings is not so clear, showing a maximum for 2 molecules/u.c. and a net decrease with higher loadings. This point reflects in some way the trend of the diffusion coefficients *versus* ethane loading.

Turning to the specific event numbers, it should be remarked that the only case in which a significant difference between  $n_s$  and  $n_z$  is present is the 500 K simulation; in all the other cases the difference is very small and cannot explain alone the diffusional anisotropy of ethane, as we already saw in Tables I and II. In other words the single-step model, when applied in this “direct” way, fails to reproduce the observed differences in the monodimensional diffusion coefficients. Indeed, looking at Eqs. (16)–(18), any difference between  $D_y$  and  $D_x$  could only arise from  $n_s > n_z$ , but we obtain  $n_s \cong n_z$  in almost all cases. On the other hand, Eqs.

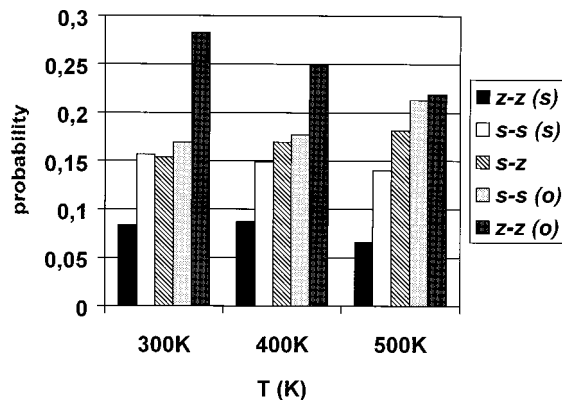


FIG. 5. Histograms of the event probabilities at different temperatures (loading = 4 molecules/u.c.).

(4)–(6) show that the anisotropy should result from a difference between the number of “double-straight” events  $n_{ss}^s$  and the number of “double-zig-zag” events  $n_{zz}^s$ , which is actually always present ( $n_{ss}^s \cong 2n_{zz}^s$ ). Therefore, the two-step model seems to work better also in the prediction of the diffusional anisotropy.

But how are the diffusion coefficients influenced by slight variations in the  $n_{zz}^s$ ,  $n_{ss}^s$  and  $n_{sw}$  numbers? From Eqs. (4)–(6), by putting  $a \cong b \cong 20$  Å, one obtains

$$\Delta r^2(t) (\text{Å}^2) \cong 400[n_{ss}^s(t) + n_{zz}^s(t)] + 245n_{sw}(t). \quad (35)$$

This equality shows that the total number of switches has a much lower weight on the overall MSD than the sum of the numbers of straight-to-straight and zigzag-to-zigzag coupled events. Actually, this sum is about six events/molecule for the 1, 2, and 4 molecules/u.c. cases, and falls to about four for the 6 molecules/u.c. loading, in which case a net decrease of the diffusion coefficient was observed. The same sum rises to  $\cong 8$  at 400 K and to  $\cong 9$  at 500 K, but also with a significant increase in  $n_{sw}$ .

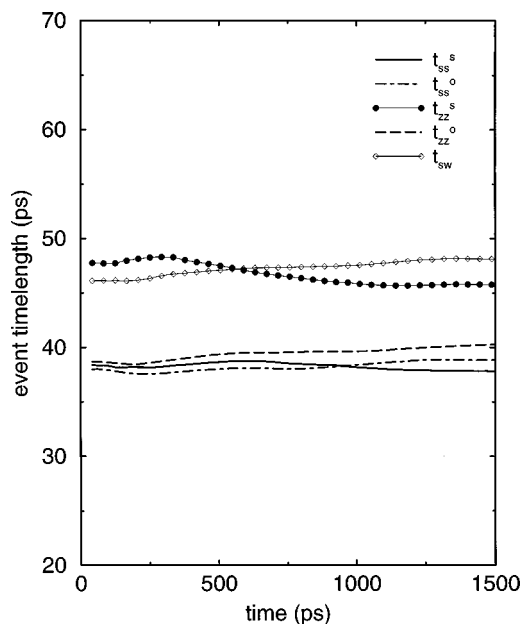


FIG. 6. Trend of the average event timelengths as a function of the time.

TABLE V. Event timelengths (ps) at different loadings.

Loading (molecule/u.c.)	$t_s$	$t_z$	$t_{ss}^s$	$t_{ss}^o$	$t_{zz}^s$	$t_{zz}^o$	$t_{sw}$	$t_{sz}$	$t_{zs}$	$t_1$	$t_2$
1	17.75	19.74	31.48	34.88	41.48	37.83	40.32	38.26	42.38	18.74	37.5
2	17.41	16.69	34.35	31.28	42.36	30.40	37.45	34.38	40.51	17.04	34.08
4	20.94	21.20	38.17	38.42	45.83	39.64	47.56	44.49	50.62	21.08	42.1
6	25.99	24.16	48.87	50.83	61.52	45.98	52.45	50.93	53.98	25.07	50.14

## B. Qualitative interpretation of the diffusional mechanism

From a general point of view, we could gain insight into the diffusional mechanism from the analysis of the event probabilities, which are not influenced by the different total number of events in the various cases. As shown in the histograms of Figs. 4 and 5, the least probable event is clearly the zigzag-to-zigzag ( $zz^s$ ) double-step *in the same direction*, while the most probable one is again the double-zigzag step, but *in opposite directions*. The general trend is

$$p_{zz}^s < p_{ss}^s \cong p_{sz} = p_{zs} \leq p_{ss}^o < p_{zz}^o$$

(note that  $p_{sw} = 2p_{sz} = 2p_{zs}$ , but a meaningful comparison should obviously be separately made with each one of the two possible switch events). Only at 500 K is a deviation from this trend observed: there, the two events connected to the “coming back” of the molecule into the starting intersection, i.e.,  $ss^o$  and  $zz^o$  happen with almost the same probability. However, it is remarkable that the general trend is almost unchanged in all cases, indicating that the diffusion mechanism should not be influenced by the different loading and temperature.

This mechanism seems to indicate that when an ethane molecule coming from a zigzag channel reaches an intersection, it will often reverse its motion, coming back to the previous intersection; on the other hand, a molecule coming from a straight channel has almost equal probabilities to continue in the same direction, to switch to a zigzag channel or to return to its starting intersection. The timelength characteristic of each event was calculated simultaneously with the event numbers: when a determinate event was found in the examination of the trajectory, its duration was also recorded; therefore the timelength of each event is also a function of the time: i.e., considering trajectory fractions of 2 ns we could find that the mean timelength of, e.g., straight-to-straight (same direction) steps is 30 ps [then  $t_{ss}^s(t_0=2\text{ ns}) = 30\text{ ps}$ ] and with a different  $t_0$  value (which will also include different intervals in the average) the same timelength may slightly vary. The time evolution of the timelengths relative to the five different two-step events for the 4 molecule/u.c., 300 K case is shown in Fig. 6. As expected,

all the curves are almost constant; however, in the following discussion we will consider the values corresponding to  $t = 1\text{ ns}$ , as for the event numbers calculation. Tables V and VI report the calculated timelengths. The overall timelength of single events was calculated as

$$t_1 = p_s t_s + p_z t_z, \quad (36)$$

while for the coupled events we have

$$t_2 = p_{ss}^s t_{ss}^s + p_{ss}^o t_{ss}^o + p_{zz}^s t_{zz}^s + p_{zz}^o t_{zz}^o + p_{sw} t_{sw}. \quad (37)$$

Obviously the relation  $t_2 = 2t_1$  is exactly obeyed. The observed trend as a function of the loading shows similar values for the overall timelengths in the 1 and 2 molecule/u.c. cases, and a net decrease going to higher loadings:  $t_2 \cong 50\text{ ps}$  for the 6 molecules/u.c. case. This trend again reflects the situation already observed for the event numbers: the 2 molecules/u.c. case presents the *highest* average number of events, and the *lowest* average event timelength. Note that this point does not necessarily lead to a greater total MSD: actually, the above averages regard *all* events, including those in opposite directions, and do not take into account the different distributions and probabilities of each event. Indeed, the two MSD curves for the 1 and 2 molecule/u.c. cases, calculated by Eqs. (4)–(6), are very close at all times. The increase of the temperature leads to the expected overall decrease of event timelengths ( $t_1$  and  $t_2$ ).

The slowest events are the switches and the zigzag-to-zigzag displacements in the same direction, in practically all cases, while the other three displacements are always 5–10 ps faster (Figs. 7 and 8). Moreover, it should be remarked that the straight-to-zigzag interchange is always significantly faster than the zigzag-to-straight one (Tables V and VI). This last observation is in agreement with previous MD simulations of butane in silicalite,<sup>18</sup> where the orientational decorrelation times of sorbate along  $x$  and  $y$  directions were calculated. There it was found that the decay time along  $x$  was significantly greater than that along  $y$ . The decay time along  $x$  is proportional to the timelength of zigzag to straight interchanges, while the straight to zigzag switch timelength determines the decay time along  $y$ ; thus the  $s$ - $z$  switch was faster as we find for ethane.

TABLE VI. Event timelengths (ps) at different temperatures.

$T$ (K)	$t_s$	$t_z$	$t_{ss}^s$	$t_{ss}^o$	$t_{zz}^s$	$t_{zz}^o$	$t_{sw}$	$t_{sz}$	$t_{zs}$	$t_1$	$t_2$
300	20.94	21.20	38.17	38.42	45.83	39.64	47.56	44.49	50.62	21.08	42.1
400	14.42	15.80	25.79	27.22	33.16	30.01	33.21	31.74	34.67	15.12	30.21
500	11.09	12.06	21.67	18.95	26.41	22.51	25.79	24.30	27.28	11.54	23.11



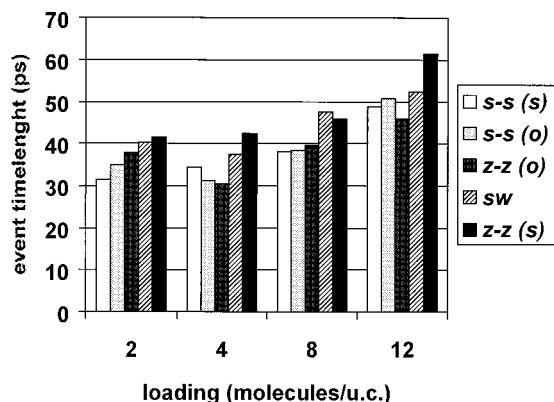


FIG. 7. Histograms of the event timelengths at different loadings ( $T = 300$  K).

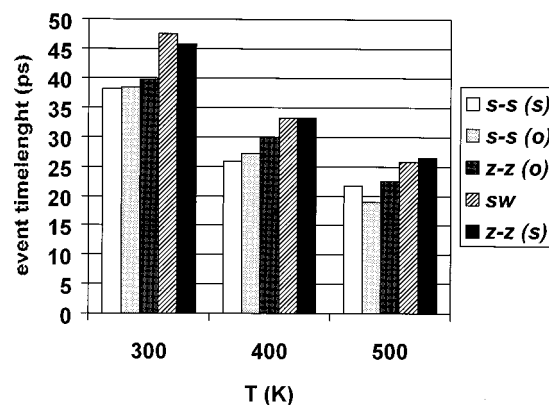


FIG. 8. Histograms of the event timelengths at different temperatures (loading=4 molecule/u.c.).

### C. Application of the modified correlation rule

In order to test the validity of the modified correlation rule, Eq. (32), the deviations of the actual two-step event numbers from their random-walk values, as expressed in Eqs. (21)–(23), need to be calculated. The “delta” values obtained from the numbers of Tables III and IV are reported in Table VII. Note that these values are differences between numbers averaged over all molecules and over all 1 ns time intervals present in the MD trajectories, so that they should be read as  $\Delta n_{zz}^s(t=1 \text{ ns})$  and so on. The largest deviations have been found for the switch events, while the displacements in the straight channels show a behavior more similar to an “uncorrelated” one. Note also that the deviations from the “theoretical” values are always negative for the  $n_{sw}$  and  $n_{zz}^s$  values, i.e., there is a lower tendency towards such kinds of events than what is expected on the hypothesis of a fast randomization of the molecular migration between intersections. Conversely, the  $\Delta n_{ss}^s$  values are always  $\geq 0$ , indicating that when a molecule moving along the  $y$  direction enters an intersection, it tends to continue in the same direction with greater probability, compared to the random case. Clearly the sum of all the deviations, including  $\Delta n_{zz}^o$  and  $\Delta n_{ss}^o$  must be close to zero

$$\begin{aligned} \Sigma \Delta &= \Delta n_{zz}^s + \Delta n_{zz}^o + \Delta n_{ss}^s + \Delta n_{ss}^o + \Delta n_{sw} \\ &= n_{zz}^s + n_{zz}^o + n_{ss}^s + n_{ss}^o + n_{sw} \\ &\quad - 2 \cdot \left(\frac{1}{4}\right) n_z^2/n - 2 \cdot \left(\frac{1}{4}\right) n_s^2/n - n_z n_s/n \\ &= n - (n_z^2 + n_s^2 + 2n_z n_s)/n = 0, \end{aligned} \quad (38)$$

where we have made use of Eq. (10) and of Eqs. (21)–(23). This entails that any deficiency (excess) of a specific kind of event will be balanced by an accompanying excess (deficiency) of another kind of event.

The results of Table VII seem to show that correlation effects are important, especially for the switches (which are much less than in the case of uncorrelated motion) and for the  $z$ - $z$  (opposite direction) events, whose number is considerably higher than the “uncorrelated” one. The question arises whether these deviations are *only* due to correlation effects; actually a few switches are observed because the molecule tends to maintain its direction of motion, in par-

ticular along  $y$ , and this is mainly a “memory” effect. At the same time, the shape of zig-zag channels determines the occurrence of many bouncing-back events, and this may be considered both a kinetic and a memory effect. In other words, although the duration of single steps ( $\sim 20$  ps, Table V) seems to be long enough to randomize the motion of a small molecule like ethane, the data of Table VII point out that the motion of ethane in silicalite is considerably influenced by memory effects.

Table VIII compares the  $D_z$  values obtained by the standard method [Eq. (34)] to those obtained by inserting the “experimental”  $D_x$  and  $D_y$  [i.e., obtained by Eq. (34)] into the correlation rule expressions, Eqs. (1) and (32). The modified correlation rule does not always predict  $D_z$  values better than the first-approximation rule, Eq. (1), but for the runs with 4 and 6 molecules/u.c. the introduction of the deviations seems to work in the right way, i.e., Eq. (32) gives  $D_z$  values closer to the right (second column) ones.

## VI. CONCLUSIONS

We attempted to illuminate the effects that the particle “memory” of its previous path may have on the overall propagation in silicalite-type zeolites. One may argue that such effects should be most important only for (relatively) long-chain alkanes, but we also found that for the ethane case they are non-negligible. Indeed, the deviations of the event numbers from their uncorrelated values (Table VII) are considerably different from zero in all cases, showing that a completely random description of the motion between intersections would be not exact.

TABLE VII. Deviations of the two-step event numbers from their theoretical (uncorrelated) values.

Loading (molecules/u.c.)	$\Delta n_{zz}^s$	$\Delta n_{ss}^s$	$\Delta n_{sw}$	$\Delta n_{zz}^o$	$\Delta n_{ss}^o$
1	-1.32	0.84	-3.92	3.28	1.12
2	-1.71	0.79	-5.67	4.54	2.03
4(300 K)	-1.25	1.01	-4.61	3.55	1.28
4(400 K)	-1.33	0.88	-5.36	4.01	1.80
4(500 K)	-1.86	-0.10	-5.88	4.8	3.04
6	-1.46	0.32	-4.17	3.55	1.75

TABLE VIII.  $D_z$  values obtained by the standard method [Eq. (34)], by the first correlation rule [Eq. (1)] and by the modified correlation rule [Eq. (32)] ( $/10^{-9} \text{ m}^2 \text{ s}^{-1}$ ).

Loading (molecules/u.c.)	$D_z$ (standard)	$D_z$ [Eq. (1)]	$D_z$ [Eq. (32)]
1	1.8	1.78	1.69
2	2.0	1.51	1.36
4(300 K)	1.2	1.54	1.32
4(400 K)	1.5	2.26	2.03
4(500 K)	2.3	2.67	2.67
6	0.7	0.84	0.79

The proposed two-step model, which takes account of such deviations, has been tested against the diffusion data obtained by the standard analysis of the MD simulation results, Eq. (34). The direct application of the two-step model to the calculation of the monodimensional MSDs, through Eqs. (4)–(6), gives considerably better results than those obtained from the “uncorrelated” Eqs. (16)–(18). The two-step model works better both in the characterization of the diffusional anisotropy and in the prediction of the total diffusion coefficient. Anyway, both models are approximated and overestimate the mean square displacements; however, since the two-step model may be considered an higher-order approximation compared to the random-walk description, it is likely that an  $N$ -step model (with  $N > 2$ ) could further improve the agreement between the theory (i.e., jump model results) and “experiment” (i.e., standard MD results, which, in turn, agree well with the measured values, see Ref. 17).

It is worth noting that the proposed probabilistic models may considerably extend the space and time scales of the standard MD results; this follows from the high linearity with time of the MSD curves obtained from the two-step model, which in turn stems from the constant-with-time ratios between the calculated  $n$  numbers. In other words, the event probabilities obtained from a direct event analysis could probably define the diffusional behavior of the molecules on very long time scales, compared to the standard analysis.

Some interesting insights into the qualitative features of the propagation have been also obtained from an analysis of

the various event probabilities and characteristic timelengths under different temperature and concentration conditions.

Finally, it has been shown that the original random correlation rule between the elements of the diffusional tensor may in some cases be improved by including the above-mentioned deviations, as calculated according to the two-step model. It is likely that the modified correlation rule could work even better when applied to the diffusion of longer-chain alkanes, in which case larger deviations from randomness than for ethane must be expected.

## ACKNOWLEDGMENTS

We are grateful to MURST, the University of Sassari, and Consiglio Nazionale delle Ricerche for financial support.

- <sup>1</sup>J. Kärger, *J. Phys. Chem.* **95**, 5558 (1991).
- <sup>2</sup>J. Kärger and H. Pfeifer, *Zeolites* **12**, 872 (1992).
- <sup>3</sup>N.-K. Bär, J. Kärger, H. Pfeifer, H. Schäfer, and W. Schmitz, *Microporous Mesoporous Mater.* **22**, 289 (1998).
- <sup>4</sup>J. Caro, M. Noack, J. Richter-Mendau, F. Marlow, D. Petersohn, M. Griepentrog, and J. Kornatowski, *J. Phys. Chem.* **97**, 13685 (1993).
- <sup>5</sup>D. M. Ruthven, M. Eic, and E. Richard, *Zeolites* **11**, 647 (1991).
- <sup>6</sup>C. L. Cavalcante, S. Brandani, and D. M. Ruthven, *Zeolites* **18**, 282 (1997).
- <sup>7</sup>U. Hong, J. Kärger, R. Kramer, H. Pfeifer, G. Seiffert, U. Müller, K. K. Müller, K. K. Unger, H.-B. Lück, and T. Ito, *Zeolites* **11**, 225 (1991).
- <sup>8</sup>U. Hong, J. Kärger, H. Pfeifer, U. Müller, and K. K. Unger, *Z. Phys. Chem. (Munich)* **173**, 225 (1991).
- <sup>9</sup>D. Fenzke and J. Kärger, *Z. Phys. D* **25**, 345 (1993).
- <sup>10</sup>S. D. Pickett, A. K. Nowak, J. M. Thomas, B. K. Peterson, J. F. P. Swift, A. K. Cheetham, C. J. J. den Ouden, B. Smit, and M. F. M. Post, *J. Phys. Chem.* **94**, 1233 (1990).
- <sup>11</sup>R. L. June, A. T. Bell, and D. N. Theodorou, *J. Phys. Chem.* **94**, 8232 (1990).
- <sup>12</sup>P. Demontis, E. S. Fois, G. B. Suffritti, and S. Quartieri, *J. Phys. Chem.* **94**, 4329 (1990).
- <sup>13</sup>E. J. Maginn, A. T. Bell, and D. N. Theodorou, *J. Phys. Chem.* **100**, 7155 (1996).
- <sup>14</sup>R. C. Runnebaum, E. J. Maginn, *J. Phys. Chem. B* **101**, 6394 (1997).
- <sup>15</sup>P. Demontis, G. B. Suffritti, S. Quartieri, E. S. Fois, and A. Gamba, *Zeolites* **7**, 522 (1987).
- <sup>16</sup>P. Demontis, G. B. Suffritti, S. Quartieri, E. S. Fois, and A. Gamba, *J. Phys. Chem.* **92**, 867 (1988).
- <sup>17</sup>P. Demontis, G. B. Suffritti, and A. Tilocca, *J. Chem. Phys.* **105**, 5586 (1996).
- <sup>18</sup>R. L. June, A. T. Bell, and D. N. Theodorou, *J. Phys. Chem.* **96**, 1051 (1992).